14

Cellular Automata as Microscopic Models of Cell Migration in Heterogeneous Environments

Haralambos Hatzikirou and Andreas Deutsch

Center for Information Services and High-Performance Computing, Technische Universität Dresden, Nöthnitzerstr. 46, 01069 Dresden, Germany

Understanding the precise interplay of moving cells with their typically heterogeneous environment is crucial for central biological processes as embryonic morphogenesis, wound healing, immune reactions or tumor growth. Mathematical models allow for the analysis of cell migration strategies involving complex feedback mechanisms between the cells and their microenvironment. Here, we introduce a cellular automaton (especially lattice-gas cellular automaton—LGCA) as a microscopic model of cell migration together with a (mathematical) tensor characterization of different biological environments. Furthermore, we show how mathematical analysis of the LGCA model can yield an estimate for the cell dispersion speed within a given environment. Novel imaging techniques like diffusion tensor imaging (DTI) may provide tensor data of biological microenvironments. As an application, we present LGCA simulations of a proliferating cell population moving in an external field defined by clinical DTI data. This system can serve as a model of *in vivo* glioma cell invasion.

I. Introduction

Alan Turing in his landmark paper of 1952 introduced the concept of self-organization to biology (Turing, 1952). He suggested "that a system of chemical substances, called morphogens, reacting together and diffusing through a tissue, is adequate to account for the main phenomena of morphogenesis. Such a system, although it may originally be quite homogeneous, may later develop a pattern or structure due to an instability of the homogeneous equilibrium, which is triggered off by random disturbances." Today, it is realized that, in addition to diffusible signals, the role of cells in morphogenesis is crucial. In particular, living cells possess migration strategies that go far beyond the merely random displacements characterizing nonliving molecules (diffusion). It has been shown that the microenvironment plays a an important role in the way that cells select their migration strategies (Friedl and Broecker, 2000). Moreover, the microenvironment provides the prototypic substrate for cell migration in embryonic morphogenesis, immune defense, wound repair or even tumor invasion.

The cellular microenvironment is a highly heterogeneous medium for cell motion including the extracellular matrix composed of fibrillar structures, collagen matrices, diffusible chemical signals as well as other mobile and immobile cells. Cells move within their environment by responding to variuos stimuli. In addition, cells change their environment locally by producing or absorbing chemicals and/or by degrading the neighboring tissue. This interplay establishes a dynamic relationship between individual cells and the surrounding substrate. In the following subsection, we provide more details about the different cell migration strategies in various environments. Environmental heterogeneity contributes to the complexity of the resulting cellular behaviors. Moreover, cell migration and interactions with the environment are taking place at different spatiotemporal scales. Mathematical modeling has proven extremely useful in getting insights into such multiscale systems. In this paper, we show how a suitable microscopical mathematical model (a cellular automaton) can contribute to understand the interplay of moving cells with their heterogeneous environment. A broad spectrum of challenging questions can be addressed, in particular:

- What kind of spatiotemporal patterns are formed by moving cells using different strategies?
- How does the moving cell population affect its environment and what is the feedback to its motion?
- What is the spreading speed of a cell population within a heterogeneous environment?

A. Types of Cell Motion

The cell migration type is strongly coupled to the kind of environment that hosts the cell population. A range of external cues impart information to the cells which regulate

Table I Diversity in cell migration strategies (after Friedl *et al.*, 2004)

Type/motion	Random Walk	Cell–Cell Adhesion	Cell–ECM Adhesion	Proteolysis
Amoeboid	++	−/+	−/+	+/−
Mesenchymal	−	−/+	+	+
Collective	−	++	++	+

In different tissue environments, different cell types exhibit either individual (amoeboid or mesenchymal) or collective migration mechanisms to overcome and integrate into tissue scaffolds (see text for explanations).

their movement, including long-range diffusible chemicals (e.g., chemoattractants), contact with membrane-bound molecules on neighboring cells (mediating cell–cell adhesion and contact inhibition) and contact with the extracellular matrix (ECM) surrounding the cells (contact guidance, haptotaxis). Accordingly, the environment can act on the cell motion in many different ways.

Recently, Friedl *et al.* (2000, 2004) have investigated in depth the kinds of observed cell movement in tissues. The main processes that influence cell motion are identified by: cell–ECM adhesion forces introducing integrin-induced motion and cell–cell adhesive forces leading to cadherin-induced motion. The different contributions of these two kinds of adhesive forces characterize the particular type of cell motion. Table I gives an overview of the possible types of cell migration in the ECM.

Amoeboid motion is the simplest kind of cell motion and can be characterized as random motion of cells without being affected by the integrin concentration of the underlying matrix. Amoeboidly migrating cells develop a dynamic leading edge rich in small pseudopodia, a roundish or ellipsoid main cell body and a trailing small uropod. Cells, like neutrophils, perceive the tissue as a porous medium, where their flexibility allows them to move through the tissue without significantly changing it. On the other hand, mesenchymal motion of cells (for instance, glioma cells) leads to alignment with the fibers of the ECM, since the cells are responding to environmental cues of nondiffusible molecules bound to the matrix and follow the underlying structure. Mesenchymal cells retain an adhesive, tissue-dependent phenotype and develop a spindle-shaped elongation in the ECM. In addition, the proteolytic activity (metalloproteinases production) of such cells allows for the remodeling of the matrix and establishes a dynamical environment. The final category is collective motion of cells (e.g., endothelial cells) that respond to cadherins and create cell–cell bounds. Clusters of cells can move through the adjacent connective tissue. Leading cells provide the migratory traction and, via cell–cell junctions, pull the following group forward.

One can think about two distinct ways of cells responding to environmental stimuli: either the cells are following a certain direction and/or the environment imposes an orientational preference leading to alignment. An example of the directed case is the graded spatial distribution of adhesion ligands along the ECM which is thought to influence the direction of cell migration (McCarthy and Furcht, 1984), a phenomenon

Table II   In this table, we classify the environmental effect with respect to different cell migration strategies

	Static	Dynamic
Direction	Haptotaxis	Chemotaxis
Orientation	Amoeboid	Mesenchymal

One can distinguish static and dynamic environments. In addition, we differentiate environments that impart directional or only orientational information for migrating cells (see text for explanations).

known as haptotaxis (Carter, 1965). Chemotaxis mediated by diffusible chemotactic signals provides a further example of directed cell motion in a dynamically changing environment. On the other hand, alignment is observed in fibrous environments where amoeboid and mesenchymal cells change their orientation according to the fiber structure. Mesenchymal cells use additionally proteolysis to facilitate their movement and remodel the neighboring tissue (dynamic environment). Table II summarizes the above statements.

It has been shown that the basic strategies of cell migration are retained in tumor cells (Friedl and Wolf, 2003). However, it seems that tumor cells can adapt their strategy, i.e., the cancer cell's migration mechanisms can be reprogrammed, allowing it to maintain its invasive properties via morphological and functional dedifferentiation (Friedl and Wolf, 2003). Furthermore, it has been demonstrated that the microenvironment is crucial for cancer cell migration, e.g., fiber tracks in the brain's white matter facilitate glioma cell motion (Swanson *et al.*, 2002; Hatzikirou *et al.*, 2005). Therefore, a better understanding of cell migration strategies in heterogeneous environments is particularly crucial for designing new cancer therapies.

B. Mathematical Models of Cell Migration

The present paper focuses on the analysis of cell motion in heterogeneous environments. A large number of mathematical models has already been proposed to model various aspects of cell motion. Reaction–diffusion equations have been used to model the phenomenology of motion in various environments, like diffusible chemicals [Keller–Segel chemotaxis model (Keller and Segel, 1971), etc.] and mechanical ECM stresses (Murray *et al.*, 1983). Integrodifferential equations have been introduced to model fiber alignment in the work of Dallon, Sherratt, and Maini (Dallon *et al.*, 2001). Navier–Stokes equations and the theory of fluid dynamics provided insight of "flow" of cells within complex environments, for instance, modeling cell motion as flow in porous media (Byrne and Preziosi, 2003). However, the previous continuous models describe cell motion at a macroscopic level neglecting the microscopical cell–cell and cell–environment interactions. Kinetic equations (Dolak and Schmeiser, 2005;

Chauviere *et al.*, 2007) and especially transport equations (Othmer *et al.*, 1988; Dickinson and Tranquillo, 1993; Dickinson and Tranquillo, 1995; Hillen, 2006) have been proposed as models of cell motion along tissues, at a mesoscopic level of description (the equations describe the behavior of cells within a small partition of space). Microscopical experimental data and the need to analyze populations consisting of a low number of cells call for models that describe the phenomena at the level of cell–cell interactions, e.g., interacting particle systems (Liggett, 1985), cellular automata (CA) (Deutsch and Dormann, 2005), off-lattice Langevin methods (Galle *et al.*, 2006; Grima, 2007; Newman and Grima, 2004), active Brownian particles (Schweitzer, 2003; Peruani and Morelli, 2007), and other microscopic stochastic models (Othmer and Stevens, 1997; Okubo and Levin, 2002).

The focus of this study is to introduce CAs, and especially a subclass of them called lattice-gas cellular automata (LGCA), as a microscopic model of cell motion (Deutsch and Dormann, 2005). LGCA (and lattice Boltzmann equation (LBE) models) have been originally introduced as discrete models of fluid dynamics (Chopard and Droz, 1998). In contrast with other CA models, LGCA allow for modeling of migrating particles in a straightforward manner (see Section II). In the following, we show that LGCA can be extended to serve as models for migrating cell populations. Additionally, their discrete nature allows for the description of the cell–cell and cell–environment interactions at the microscopic level of single cells but at the same time enables us to observe the macroscopical evolution of the whole population.

C. Overview of the Paper

In this paper, we will explore the role of the environment (both in a directional and orientational sense) for cell movement. Moreover, we consider cells that lack metalloproteinase production (proteolytic proteins) and do not change the ECM structure, introducing static environments (additionally, we do not consider diffusible environments). Moreover, we will consider populations with a constant number of cells (no proliferation/death of cells) in time.

In Section II, we introduce the modeling framework of CA and particularly LGCA. In Section III, we define LGCA models of moving cells in different environments that impart directional and orientational information to the moving cells. Furthermore, we provide a tensor characterization for the environmental impact on migrating cell populations. As an example, we present simulations of a proliferative cell population in a tensor field defined by clinical DTI data. This system can serve as a model of *in vivo* glioma cell invasion. In Section IV, we show how mathematical analysis of the LGCA model can yield an estimate for the cell dispersion speed within a given environment. Finally, in Section V, we sum up the results, we critically argue on the advantages and disadvantages of using LGCA, and we discuss potential venues for analysis, extensions and applications.
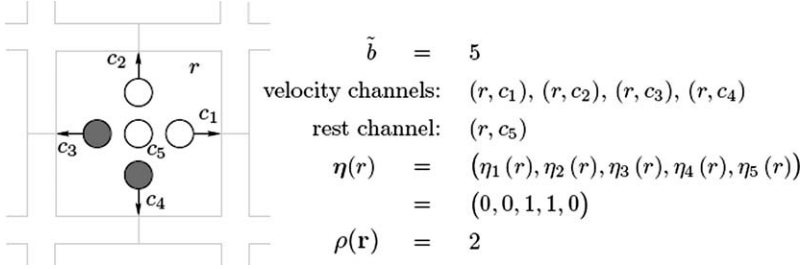
$$\tilde{b} = 5$$
$$\text{velocity channels:} \quad (r, c_1), (r, c_2), (r, c_3), (r, c_4)$$
$$\text{rest channel:} \quad (r, c_5)$$
$$\eta(r) = (\eta_1(r), \eta_2(r), \eta_3(r), \eta_4(r), \eta_5(r))$$
$$= (0, 0, 1, 1, 0)$$
$$\rho(\mathbf{r}) = 2$$

Figure 1   Node configuration: channels of node r in a two-dimensional square lattice ($b = 4$) with one rest channel ($\beta = 1$). Gray dots denote the presence of a particle in the respective channel.

Figure 2   Example for interaction of particles at two-dimensional square lattice node r; gray dots denote the presence of a particle in the respective channel. No confusion should arise by the arrows indicating channel directions.

II. Idea of the LGCA Modeling Approach

The strength of the lattice-gas method lies in its potential to unravel effects of movement and interaction of individuals (e.g., cells). In traditional cellular automaton models implementing movement of individuals is not straightforward, as one node in the lattice can typically only contain one individual, and consequently movement of individuals can cause collisions when two individuals want to move into the same empty node. In a lattice-gas model this problem is avoided by having separate channels for each direction of movement. The channels specify the direction and magnitude of movement, which may include zero velocity (resting) states. For example, a square lattice has four nonzero velocity channels and an arbitrary number of rest channels (Fig. 1). Moreover, LGCA impose an exclusion principle on channel occupation, i.e. each channel may at most host one particle.

The transition rule of a LGCA can be decomposed into two steps. An *interaction* step updates the state of each channel at each lattice site. Particles may change their velocity state and appear or disappear (birth/death) as long as they do not violate the exclusion principle (Fig. 2). In the *propagation* step, cells move synchronously in the direction and by the distance specified by their velocity state (Fig. 3). The propagation step is deterministic and conserves mass and momentum. Synchronous transport prevents particle collisions which would violate the exclusion principle (other models
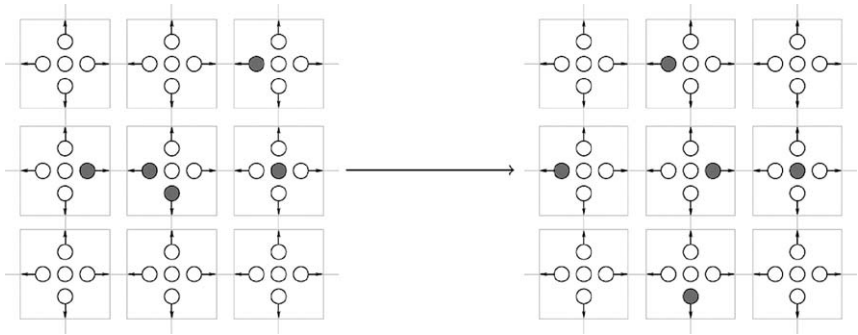
Figure 3 Propagation in a two-dimensional square lattice with speed $m = 1$; lattice configurations before and after the propagation step; gray dots denote the presence of a particle in the respective channel.
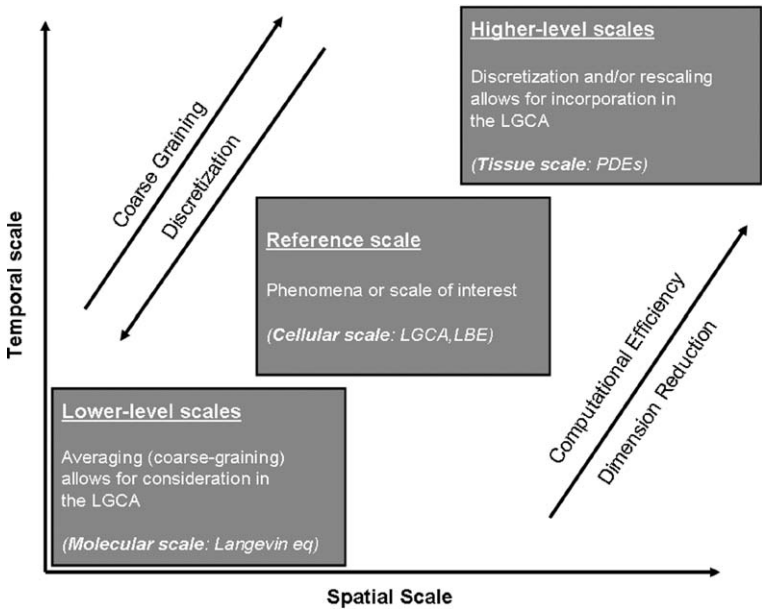

Figure 4 The sketch visualizes the hierarchy of scales relevant for the LGCA models introduced in this chapter (see text for details).

have to define a collision resolution algorithm). LGCA models allow parallel synchronous movement and updating of a large number of particles.

The basic idea of lattice-gas automaton models is to mimic complex dynamical system behavior by the repeated application of simple local migration and interaction rules. The reference scale (Fig. 4) of the LGCA models introduced in this chapter is

that of a finite set of cells. The dynamics evolving at smaller scales (intracellular) are included in a coarse-grained manner, by introducing an appropriate stochastic interaction rule. This means that our lattice-gas automata impose a microscopic, though not truly molecular, view of the system by conducting fictive microdynamics on a regular lattice. Please note that the theoretically inclined reader can find, in Appendix A, a detailed definition of the LGCA mathematical nomenclature (after Deutsch and Dormann, 2005).

III. LGCA Models of Cell Motion in a Static Environment

In this section, we define two LGCA models that describe cell motion in static environments. We especially address two problems:

- How can we model the environment?
- How should the automaton rules be chosen to model cell motion in a specific environment?

As we already stated, we want to mathematically model biologically relevant environments. According to Table II, we distinguish a "directional" and an "orientational" environment, respectively. The mathematical entity that allows for the modeling of such environments is called a *tensor field*. A tensor field is a collection of different tensors which are distributed over a spatial domain. A *tensor* is (in an informal sense) a generalized linear 'quantity' or 'geometrical entity' that can be expressed as a multidimensional array relative to a choice of basis of the particular space on which the tensor is defined. The intuition underlying the tensor concept is inherently geometrical: a tensor is independent of any chosen frame of reference.

The rank of a particular tensor is the number of array indices required to describe it. For example, mass, temperature, and other scalar quantities are tensors of rank 0; while force, momentum, velocity and further vector-like quantities are tensors of rank 1. A linear transformation such as an anisotropic relationship between velocity vectors in different directions (diffusion tensors) is a tensor of rank 2. Thus, we can represent an environment with directional information as a vector (tensor of rank 1) field. The geometric intuition for a vector field corresponds to an 'arrow' attached to each point of a region, with variable length and direction (Fig. 5). The idea of a vector field on a curved space is illustrated by the example of a weather map showing wind velocity, at each point of the earth's surface. An environment that carries orientational information for each geometrical point can be modeled by a tensor field of rank 2. A geometrical visualization of a second order tensor field can be represented as a collection of ellipsoids, assigned to each geometrical point (Fig. 6). The ellipsoids represent the orientational information that is encoded into tensors.

To model cell motion in a given tensor field (environment)—of rank 1 or 2—we should modify the interaction rule of the LGCA. We use a special kind of interaction
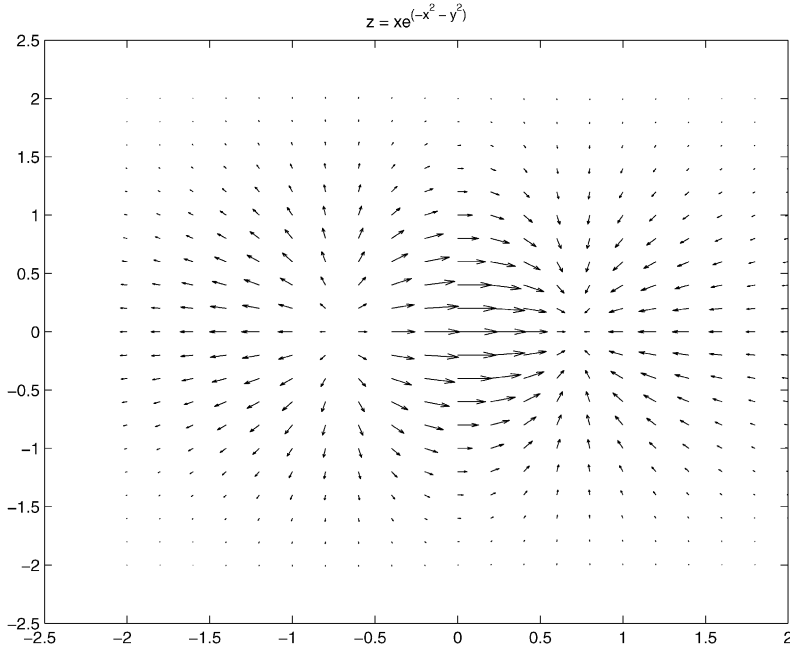
$$z = xe^{(-x^2 - y^2)}$$

Figure 5 An example of a vector field (tensor field of rank 1). The vectors (e.g., integrin receptor density gradients) show the direction and the strength of the environmental drive.

rules for the LGCA dynamics, firstly introduced by Alexander *et al.* (1992). We consider biological cells as random walkers that are reoriented by maximizing a potential-like term. Assuming that the cell motion is affected by cell–cell and cell–environment interactions, we can define the potential as the sum of these two interactions:

$$G(r, k) = \sum_j G_j(r, k) = G_{cc}(r, k) + G_{ce}(r, k), \tag{1}$$

where $G_j(r, k)$, $j = $ cc, ce is the subpotential that is related to cell–cell and cell–environment interactions, respectively.

Interaction rules are formulated in such a way that cells preferably reorient into directions which maximize (or minimize) the potential, that is according to the gradients of the potential $G'(r, k) = \nabla G(r, k)$.

Consider a lattice-gas cellular automaton defined on a two-dimensional lattice with b velocity channels ($b = 4$ or $b = 6$). Let the number of particles at node r at time k be denoted by

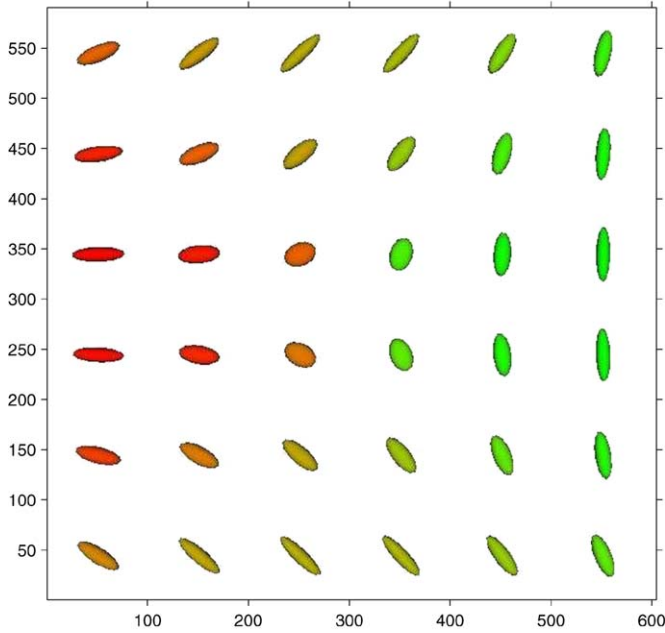$$\rho(r, k) = \sum_{i=1}^{\tilde{b}} \eta_i(r, k),$$

Figure 6 An example of a tensor field (tensor field of rank 2). We represent the local information of the tensor as ellipsoids. The ellipsoids can encode, e.g., the degree of alignment of a fibrillar tissue. The colors are denoting the orientation of the ellipsoids. See color insert.

and the *flux* be denoted by

$$\mathbf{J}\big(\boldsymbol{\eta}(r,k)\big) = \sum_{i=1}^{b} \mathbf{c}_i \eta_i(r,k).$$

The probability that η^C is the outcome of an interaction at node r is defined by

$$P\big(\boldsymbol{\eta} \to \boldsymbol{\eta}^C | G(r,k)\big) = \frac{1}{Z} \exp\big[\alpha F\big(G'(r,k), \mathbf{J}(\boldsymbol{\eta}^C)\big)\big]\delta\big(\rho(r,k), \rho^C(r,k)\big), \quad (2)$$

where η is the preinteraction state at r and the Kronecker's δ assumes the mass conservation of this operator. The sensitivity is tuned by the parameter α. The normalization factor is given by

$$Z = Z\big(\boldsymbol{\eta}(r,k)\big) = \sum_{\eta^C \in \mathcal{E}} \exp\big[\alpha F\big(G'(r,k), \mathbf{J}(\boldsymbol{\eta}^C)\big)\big]\delta\big(\rho(r,k), \rho^C(r,k)\big).$$

$F(\cdot)$ is a function that defines the effect of the G' gradients on the new configuration. A common choice of $F(\cdot)$ is the inner product $\langle, \rangle$, which favors (or penalizes) the

configurations that tend to have the same (or inverse) direction of the gradient G'. Accordingly, the dynamics are fully specified by the following microdynamical equation

$$\eta_i(r + \mathbf{c}_i, k + 1) = \eta_i^{\mathrm{C}}(r, k).$$

In the following, we present two stochastic potential-based interaction rules that correspond to the motion of cells in a vector field and a rank 2 tensor field, respectively. We exclude any other cell–cell interactions and we consider that the population has a fixed number of cells (mass conservation).

A. Model I

The first rule describes cell motion in a static environment that carries directional information expressed by a vector field $\mathbf{E}$. Biologically relevant examples are the motion of cells that respond to fixed integrin concentrations along the ECM (haptotaxis). The spatial concentration differences of integrin proteins constitute a gradient field that creates a kind of "drift" $\mathbf{E}$ (Dickinson and Tranquillo, 1993). We choose a two-dimensional LGCA without rest channels and the stochastic interaction rule of the automaton follows the definition of the potential-based rules [Eq. (1) with $\alpha = 1$]:

$$P(\boldsymbol{\eta} \rightarrow \boldsymbol{\eta}^{\mathrm{C}})(r, k) = \frac{1}{Z} \exp\big(\langle \mathbf{E}(r), \mathbf{J}(\boldsymbol{\eta}^{\mathrm{C}}(r, k)) \rangle\big) \delta\big(\rho(r, k), \rho^{\mathrm{C}}(r, k)\big). \tag{3}$$

We simulate our LGCA for spatially homogeneous fields $\mathbf{E}$ for various intensities and directions. In Fig. 7, we observe the time evolution of a cell cluster under the influence of a given field. We see that the cells collectively move in the gradient direction and they roughly keep the shape of the initial cluster. The simulations in Fig. 8 show the evolution of the system for different fields. It is evident that the "cells" follow the direction of the field and their speed responds positively to an increase of the field intensity.

B. Model II

We now focus on cell migration in environments that promote alignment (orientational changes). Examples of such motion are provided by neutrophil or leukocyte movement through the pores of the ECM, the motion of cells along fibrillar tissues or the motion of glioma cells along fiber track structures. As stated before, such an environment can be modeled by the use of a second rank tensor field that introduces a spatial anisotropy along the tissue. In each point, a tensor (i.e., a matrix) informs the cells about the local orientation and strength of the anisotropy and proposes a principle (local) axis of movement. For instance, the brain's fiber tracks impose a spatial anisotropy and their degree of alignment affects the strength of anisotropy.
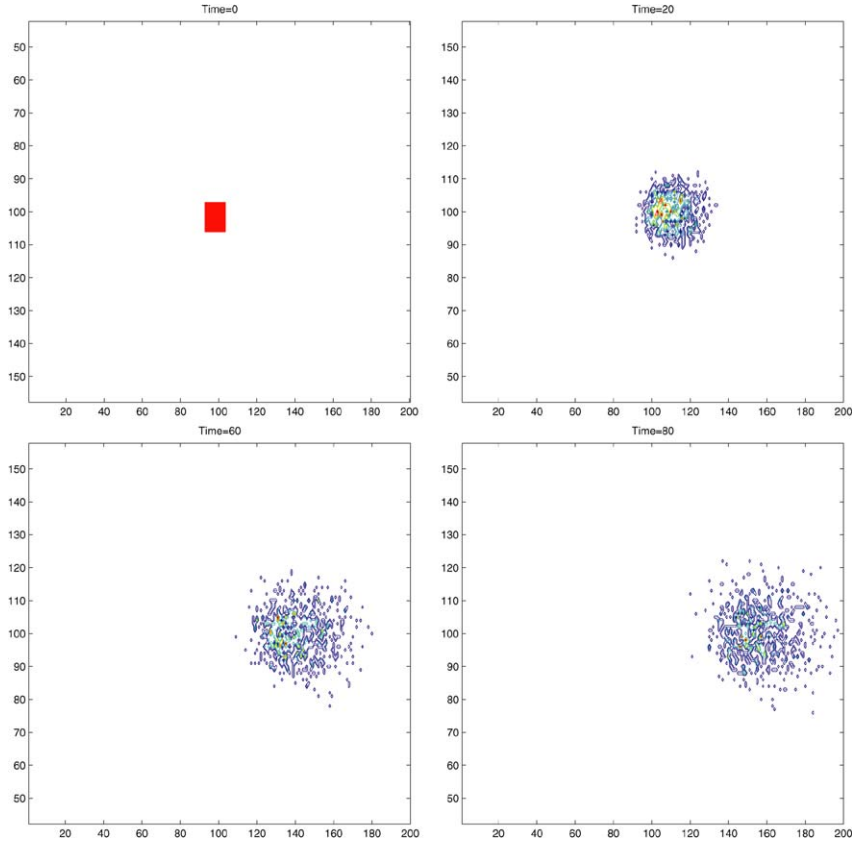
Figure 7   Time evolution of a cell population under the effect of a field $E = (1, 0)$. One can observe that the environmental drive moves all the cells of the cluster into the direction of the vector field. The blue color stands for low, the yellow for intermediate and red for high densities. See color insert.

Here, we use the information of the principal eigenvector of the diffusion tensor which defines the local principle axis of cell movement. Thus, we end up again with a vector field but in this case we exploit only the orientational information of the vector. The new rule for cell movement in an "oriented environment" is:

$$P\big(\boldsymbol{\eta} \to \boldsymbol{\eta}^{C}\big)(r, k) = \frac{1}{Z} \exp\big(|\langle \mathbf{E}(r), \mathbf{J}\big(\boldsymbol{\eta}^{C}(r, k)\big)\rangle|\big)\delta\big(\rho(r, k), \rho^{C}(r, k)\big). \qquad (4)$$

In Fig. 9, we show the time evolution of a simulation of model II for a given field. Fig. 10 shows the typical resulting patterns for different choices of tensor fields. We observe that the anisotropy leads to the creation of an ellipsoidal pattern, where the length of the main ellipsoid's axis correlates positively with the anisotropy strength.
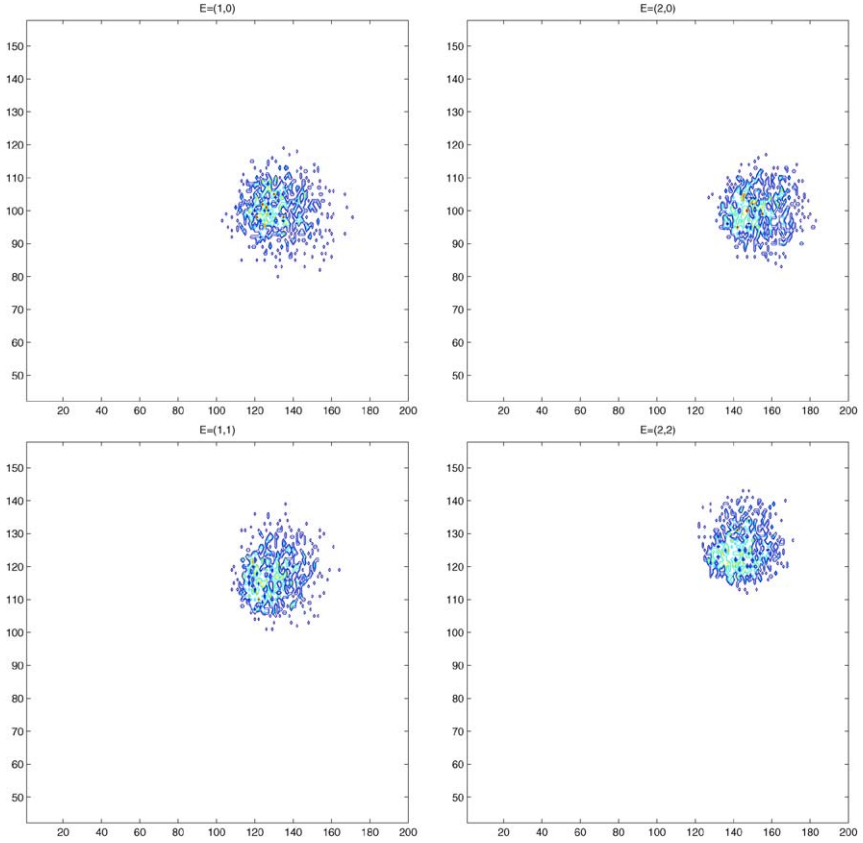
Figure 8 The figure shows the evolution of the cell population under the influence of different fields (100 time steps). Increasing the strength of the field, we observe that the cell cluster is moving faster in the direction of the field. This behavior is characteristic of a haptotactically moving cell population. The initial condition is a small cluster of cells in the center of the lattice. Colors denote different node densities (as in Fig. 7). See color insert.

This rule can, for example, be used to model the migration of glioma cells within the brain. Glioma cells tend to spread faster along fiber tracks. Diffusion Tensor Imaging (DTI) is a MRI-based method that provides the local anisotropy information in terms of diffusion tensors. High anisotropy points belong to the brain's white matter, which consists of fiber tracks. A preprocessing of the diffusion tensor field can lead to the principle eigenvectors' extraction of the diffusion tensors, that provides us with the local principle axis of motion. By considering a proliferative cell population, as in Hatzikirou *et al.* (2007), and using the resulting eigenvector field we can model and simulate glioma cell invasion. In Fig. 11, we simulate an example of
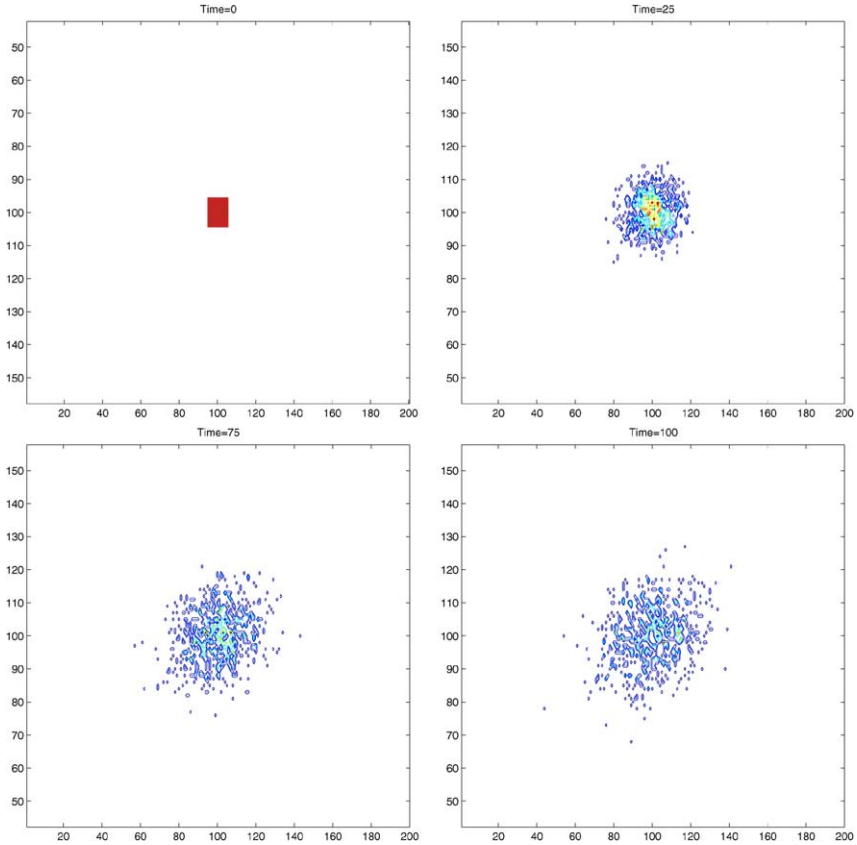
Figure 9   Time evolution of a cell population under the effect of a tensor field with principal eigenvector (principal orientation axis) $E = (2, 2)$. We observe cell alignment along the orientation of the axis defined by E, as time evolves. Moreover, the initial rectangular shape of the cell cluster is transformed into an ellipsoidal pattern with principal axis along the field **E**. Colors denote the node density (as in Fig. 7). See color insert.

glioma growth and show the effect of fiber tracks in tumor growth using the DTI information.

IV. Analysis of the LGCA Models

In this section, we provide a theoretical analysis of the proposed LGCA models. Our aim is to calculate the equilibrium cell distribution and to estimate the speed of cell dispersion under environmental variations. Finally, we compare our theoretical results with the simulations.
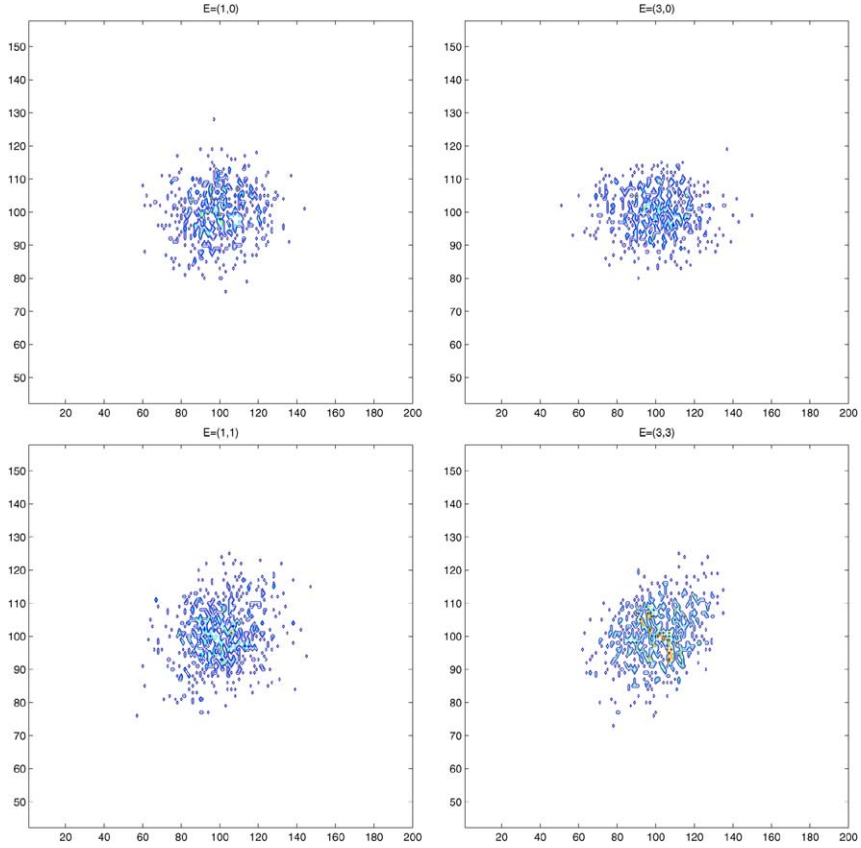
Figure 10 In this graph, we show the evolution of the pattern for four different tensor fields (100 time steps). We observe the elongation of the ellipsoidal cell cluster when the strength is increased. Above each figure the principal eigenvector of the tensor field is denoted. The initial conditions is always a small cluster of cells in the center of the lattice. The colors denote the density per node (as in Fig. 7). See color insert.

A. Model I

In this subsection, we analyze model I and we derive an estimate of the cell spreading speed in dependence of the environmental field strength. The first idea is to choose a macroscopically accessible observable that can be measured experimentally. A reasonable choice is the mean lattice flux $\langle \mathbf{J}(\eta^C) \rangle_{\mathbf{E}}$, which characterizes the mean motion of the cells, with respect to changes of the field's strength $|\mathbf{E}|$:

$$\langle \mathbf{J}(\eta^C) \rangle_{\mathbf{E}} = \sum_i \mathbf{c}_i f_i^{\text{eq}}, \tag{5}$$
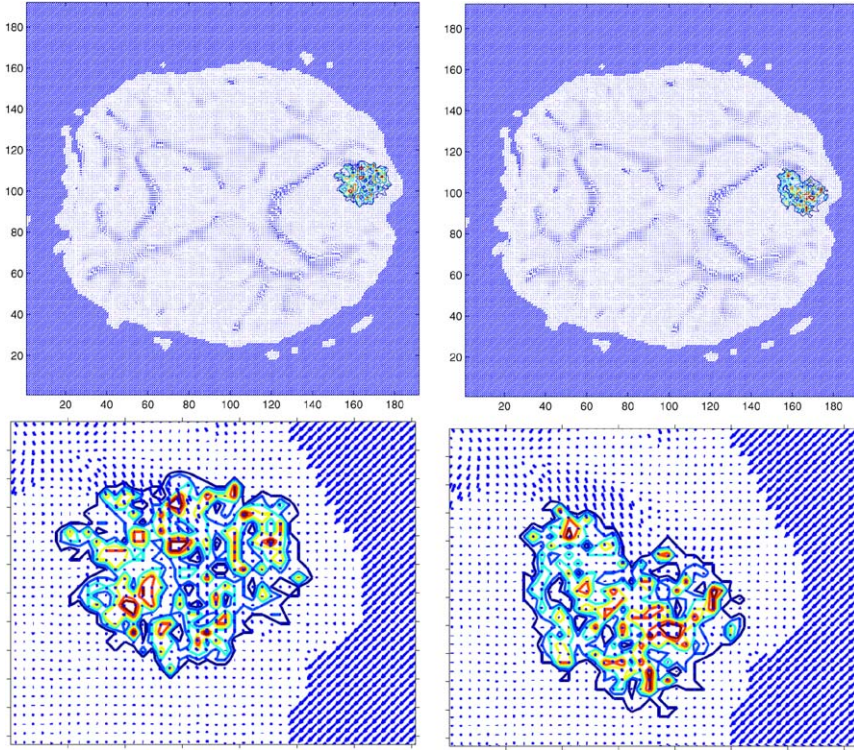
Figure 11 We show the brain's fiber track effect on glioma growth. We use a LGCA of a proliferating cancer cell population (for definition see Hatzikirou *et al.*, 2007) moving in a tensor field provided by clinical DTI data, representing the brain's fiber tracks. (Top) The left figure is a simulation without any environmental information (only diffusion). In the top right figure the effect of the fiber tracks in the brain on the evolution of the glioma growth is obvious. (Bottom) The two figures display magnification of the tumor area in the simulations above. This is an example of how environmental heterogeneity affects cell migration (in this case tumor cell migration). See color insert.

where $f_i^{\text{eq}}, i = 1, \ldots, b$ is the equilibrium density distribution of each channel. Mathematically, this is the mean flux *response* to changes of the external vector field $\mathbf{E}$. The quantity that measures the linear response of the system to the environmental stimuli is called *susceptibility*:

$$\chi = \frac{\partial \langle \mathbf{J} \rangle_{\mathbf{E}}}{\partial \mathbf{E}}. \tag{6}$$

It appears if we expand the mean flux in terms of small fields as

$$\langle \mathbf{J} \rangle_{\mathbf{E}} = \langle \mathbf{J} \rangle_{\mathbf{E}=\mathbf{0}} + \frac{\partial \langle \mathbf{J} \rangle_{\mathbf{E}}}{\partial \mathbf{E}} \mathbf{E} + O(\mathbf{E}^2). \tag{7}$$

For the zero-field case, the mean flux is zero since the cells are moving randomly within the medium (diffusion). Accordingly, for small fields $\mathbf{E} = \binom{e_1}{e_2}$ the linear approximation reads

$$\langle \mathbf{J} \rangle_{\mathbf{E}} = \frac{\partial \langle \mathbf{J} \rangle_{\mathbf{E}}}{\partial \mathbf{E}} \mathbf{E}.$$

The *general linear response relation* is

$$\left\langle \mathbf{J}(\eta^C) \right\rangle_{\mathbf{E}} = \chi_{\alpha\beta} e_\beta = \chi e_\alpha, \tag{8}$$

where the second rank tensor $\chi_{\alpha\beta} = \chi \delta_{\alpha\beta}$ is assumed to be isotropic. In biological terms, we want to study the response of cell motion with respect to changes of the spatial distribution of the integrin concentration along the ECM, corresponding to changes in the resulting gradient field.

The aim is to estimate the stationary mean flux for fields $\mathbf{E}$. At first, we have to calculate the equilibrium distribution that depends on the external field. The external drive breaks down the detailed balance (DB) conditions[1] that would lead to a Gibbs equilibrium distribution. In the case of nonzero external field, the system is as out of equilibrium. The external field (environment) induces a breakdown of the spatial symmetry which leads to nontrivial equilibrium distributions depending on the details of the transition probabilities. The (Fermi) exclusion principle allows us to assume that the equilibrium distribution follows a kind of Fermi–Dirac distribution (Frisch *et al.*, 1987):

$$f_i^{\text{eq}} = \frac{1}{1 + e^{x(\mathbf{E})}}, \tag{9}$$

where $x(\mathbf{E})$ is a quantity that depends on the field $\mathbf{E}$ and the mass of the system (if the DB conditions were fulfilled, the argument of the exponential would depend only on the invariants of the system). Thus, one can write the following *ansatz*:

$$x(\mathbf{E}) = h_0 + h_1 \mathbf{c}_i \mathbf{E} + h_2 \mathbf{E}^2. \tag{10}$$

After some algebra (the details can be found in Appendix A), for small fields $\mathbf{E}$, one finds that the equilibrium distribution looks like:

$$f_i^{\text{eq}} = d + d(d-1)h_1 \mathbf{c}_i \mathbf{E} + \frac{1}{2} d(d-1)(2d-1) h_1^2 \sum_\alpha c_{i\alpha}^2 e_\alpha^2$$

$$+ d(d-1) h_2 \mathbf{E}^2, \tag{11}$$

---

[1] The detailed balance (DB) and the semidetailed balance (SDB) imposes the following condition for the microscopic transition probabilities: $P(\eta \to \eta^C) = P(\eta^C \to \eta)$ and $\forall \eta^C \in \mathcal{E} : \sum_\eta P(\eta \to \eta^C) = 1$. Intuitively, the DB condition means that the system jumps to a new microconfiguration and comes back to the old one with the same probability (mircoreversibility). The relaxed SDB does not imply this symmetry. However, SDB guarantees the existence of steady states and the sole dependence of the Gibbs steady state distribution on the invariants of the system (conserved quantities).

where $d = \rho/b$ and $\rho = \sum_{i=1}^{b} f_i^{eq}$ is the mean node density (which coincides with the macroscopic cell density) and the parameters h_1, h_2 have to be determined. Using the mass conservation condition, we find a relation between the two parameters (see Appendix A):

$$h_2 = \frac{1-2d}{4}h_1^2. \tag{12}$$

Finally, the equilibrium distribution can be explicitly calculated for small driving fields:

$$f_i^{eq} = d + d(d-1)h_1\mathbf{c}_i\mathbf{E} + \frac{1}{2}d(d-1)(2d-1)h_1^2 Q_{\alpha\beta}e_\alpha e_\beta, \tag{13}$$

where $Q_{\alpha\beta} = c_{i\alpha}c_{i\beta} - \frac{1}{2}\delta_{\alpha\beta}$ is a second order tensor.

If we calculate the mean flux, using the equilibrium distribution up to first order terms of $\mathbf{E}$, we obtain from Eq. (5) the linear response relation:

$$\langle \mathbf{J}(\eta^C) \rangle = \sum_i c_{i\alpha} f_i^{eq} = \frac{b}{2}d(d-1)h_1\mathbf{E}. \tag{14}$$

Thus, the susceptibility reads:

$$\chi = \frac{1}{2}bd(d-1)h_1 = -\frac{1}{2}bg_{eq}h_1, \tag{15}$$

where $g_{eq} = f_i^{eq}(1-f_i^{eq})$ is the equilibrium single particle fluctuation. In Bussemaker (1996), the equilibrium distribution is directly calculated from the nonlinear lattice Boltzmann equation corresponding to a LGCA with the same rule for small external fields. In the same work, the corresponding susceptibility is determined and this result coincides with ours for $h_1 = -1$. Accordingly, we consider that $h_1 = -1$ in the following.

Our method allows us to proceed beyond the linear case, since we have explicitly calculated the equilibrium distribution of our LGCA:

$$f_i^{eq} = \frac{1}{1 + \exp\{\ln(\frac{1-d}{d}) - \mathbf{c}_i\mathbf{E} + \frac{1-2d}{4}\mathbf{E}^2\}} \longrightarrow 1 + \exp\{\ldots\}. \tag{16}$$

Using the definition of the mean lattice flux Eq. (5), we can obtain a good theoretical estimation for larger values of the field. Fig. 12 shows the behavior of the system's normalized flux obtained by simulations and a comparison with our theoretical findings. For small values of the field intensity $|\mathbf{E}|$ the linear approximation performs rather well and for larger values the agreement of our nonlinear estimate with the simulated values is more than satisfactory. One observes that the flux response to large fields saturates. This is a biologically justified result, since the speed of cells is finite and an infinite increase of the field intensity should not lead to infinite fluxes (the mean flux is proportional to the mean velocity). Experimental findings in systems of cell migration mediated by
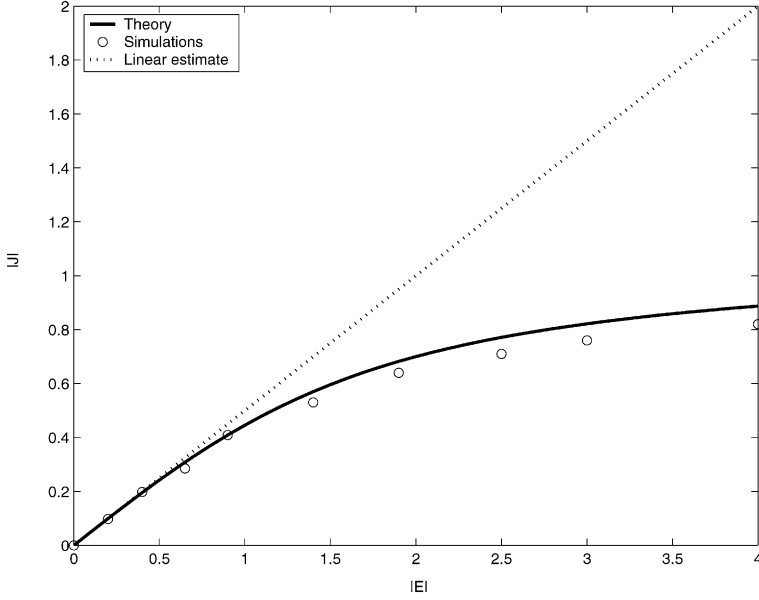
Figure 12 This figure shows the variation of the normalized measure of the total lattice flux $|\mathbf{J}|$ against the field intensity $|\mathbf{E}|$. We compare the simulated values with the theoretical calculations (for the linear and nonlinear theory). We observe that the linear theory predicts the flux strength for low field intensities. Using the full distribution, the theoretical flux is close to the simulated values also for larger field strengths.

adhesion receptors, such as ECM integrins, support the model's behavior (Palecek *et al.*, 1997; Zaman *et al.*, 2006). One could propose and analyze more observables related to the cell motion, e.g., mean square displacement, but this is beyond the scope of the paper. Here we aim to outline examples of typical analysis and not to reproduce the full repertoire of LGCA analysis for such problems.

B. Model II

In the following section, our analysis characterizes cell motion by a different measurable macroscopic variable and provides an estimate of the cell dispersion for model II. In this case, it is obvious that the average flux, defined in (5), is zero (due to the symmetry of the interaction rule). In order to measure the anisotropy, we introduce the flux difference between $\mathbf{v}_1$ and $\mathbf{v}_2$, where the $\mathbf{v}_i$'s are eigenvectors of the anisotropy matrix (they are linear combinations of $\mathbf{c}_i$'s). For simplicity of the calculations, we consider $b = 4$ and X–Y anisotropy. We define:

$$\left| \langle \mathbf{J}_{\mathbf{v}_1} \rangle - \langle \mathbf{J}_{\mathbf{v}_2} \rangle \right| = \left| \langle \mathbf{J}_{x^+} \rangle - \langle \mathbf{J}_{y^+} \rangle \right| = \left| c_{11} f_1^{\text{eq}} - c_{22} f_2^{\text{eq}} \right|. \tag{17}$$

As before, we expand the equilibrium distribution around the field $\mathbf{E}$ and we obtain Eq. (28) (see Appendix A). With similar arguments as for the previous model I, we can assume that the equilibrium distribution follows a kind of Fermi–Dirac distribution (compare with Eq. (9)). This time our *ansatz* has the following form,

$$x(\mathbf{E}) = h_0 + h_1 |\mathbf{c}_i \mathbf{E}| + h_2 \mathbf{E}^2, \tag{18}$$

because the rule is symmetric under the rotation $\mathbf{c}_i \to -\mathbf{c}_i$. Conducting similar calculations (Appendix B) as in the previous subsection, one can derive the following expression for the equilibrium distribution:

$$f_i^{\text{eq}} = d + d(d-1)h_1|\mathbf{c}_i\mathbf{E}| + \frac{1}{2}d(d-1)(2d-1)h_1^2 \sum_\alpha c_{i\alpha}^2 e_\alpha^2$$
$$+ d(d-1)(2d-1)h_1^2|c_{i\alpha}c_{i\beta}|e_\alpha e_\beta + d(d-1)h_2\mathbf{E}^2. \tag{19}$$

In Appendix B, we identify a relation between h_1 and h_2 using the microscopic mass conservation law. To simplify the calculations we assume a square lattice (similar calculations can also be carried out for the hexagonal lattice case) and using $c_{11} = c_{22} = 1$, we derive the difference of fluxes along the X–Y axes (we restrict ourselves here to the linear approximation):

$$\left| f_1^{\text{eq}} - f_2^{\text{eq}} \right| = d(d-1)h_1 \left| \sum_\alpha |c_{1\alpha}|e_\alpha - \sum_\alpha |c_{2\alpha}|e_\alpha \right| = d(d-1)h_1|e_1 - e_2|. \tag{20}$$

We observe that the parameter h_1 is still free and we should find a way to calculate it. In Appendix C, we use a method similar to the work of Bussemaker (Bussemaker, 1996) and we find that $h_1 = -1/2$. Substituting this value into the last relation and comparing with simulations (Fig. 13), we observe again a very good agreement between the linear approximation and the simulations.

V. Results and Discussion

In this study, our first goal was to interpret in mathematical terms the environment related to cell migration. We have distinguished both static and dynamic environments, depending on the interactions with the cell populations. Mathematical entities called tensors enable us to extract local information about the local geometrical structure of the tissue. Technological advances, like DTI (diffusion tensor imaging), in image analysis allow us to identify the microstructure of *in vivo* tissues. The knowledge of the microenvironment gives us a detailed picture of the medium through which the cells move, at the cellular length scale. Microscopical models are able to exploit this microscaled information and capture the dynamics.

To study and analyze the effects of the microenvironment on cell migration, we have introduced a microscopical modeling method called LGCA. We have identified and modeled the two main effects of static environments on cell migration:
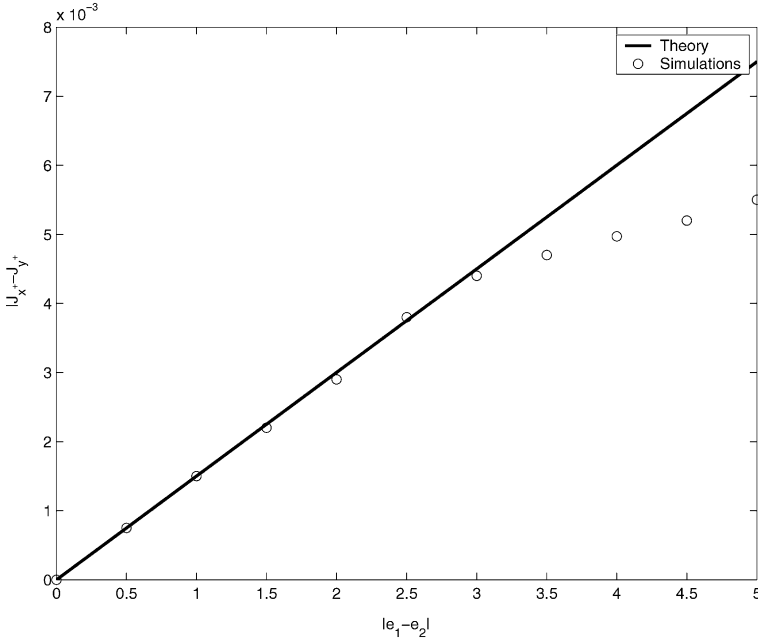
Figure 13 The figure shows the variation of the $X-Y$ flux difference against the anisotropy strength (according to model II). We compare the simulated values with the linear theory and observe a good agreement for low field strength. The range of agreement, in the linear theory, is larger than in the case of model I.

- The first model addresses motion in an environment providing directional information. Such environments can be mediated by integrin density gradient fields or diffusible chemical signals leading to haptotactical or chemotactical movement, respectively. We have carried out simulations for different static fields, in order to understand the environmental effect on pattern formation. The main conclusion is that such an environment favors the collective motion of the cells in the direction of the gradients. Interestingly, we observe in Fig. 7 that the cell population coarsely keeps the shape of the initial cluster and moves towards the same direction. This suggests that collective motion is not necessary an alternative cell migration strategy, as described in (Friedl, 2004). According to our results, collective motion can be interpreted as emergent behavior in a population of amoeboidly moving cells in a directed environment. Finally, we have calculated theoretically an estimator of the cell spreading speed, i.e., the mean flux for variations of the gradient field strength. The results exhibit a positive response of the cell flux to increasing field strength. The saturation of the response for large stimulus emphasizes the biological relevance of the model.
- The second model describes cell migration in an environment that influences the orientation of the cells (e.g., alignment). Fibrillar ECMs induce cell alignment and

can be considered as an example of an environment that affects cell orientation. Simulations show that such motion produces alignment along a principal orientation (i.e., fiber) and the cells tend to disperse along it (Fig. 9). Like model I, we have calculated the cell response to variations of the field strength, in terms of the flux difference between the principal axis of motion and its perpendicular. This difference gives us an estimate of the speed and the direction of cell dispersion. Finally, we observe a similar saturation plateau for large fields, as in model I. Moreover, we gave an application of the second model for the case of brain tumor growth using DTI data (Fig. 11).

As we have shown, the environment can influence cell motion in different ways. An interesting observation is that directional movement favors collective motion in the direction imposed by the environment. In contrast, model II imposes diffusion of cells along a principal axis of anisotropy and leads to dispersion of the cells. For both models, the cells respond positively to an increase of the field strength and their response saturates for infinitely large drives.

In the following discussion we focus on a critical evaluation of the modeling potential of lattice-gas cellular automata suggested in this paper as models of a migrating cell population in heterogeneous environments. Firstly, we discuss the advantages of the method:

- The LGCA rules can mimic the microscopic processes at the cellular level (coarse-grained subcellular dynamics). Here we focused on the analysis of two selected microscopic interaction rules. Moreover, we showed that with the help of methods motivated by statistical mechanics, we can estimate the macroscopic behavior of the whole population (e.g., mean flux).

- The discrete nature of the LGCA can be extremely useful for deeper investigations of the boundary layer of the cell population. Recent research by Bru et al. (Bru et al., 2003) has shown that the fractal properties of tumor surfaces (calculated by means of fractal scaling analysis) can provide new insights for a deeper understanding of the cancer phenomenon. In a forthcoming paper by De Franciscis et al. (De Franciscis et al., 2007), we give an example of the surface dynamics analysis of a LGCA model for tumor growth.

- Motion through heterogeneous media involves phenomena at various spatial and temporal scales. These cannot be captured in a purely macroscopic modeling approach. In macroscopic models of heterogeneous media diffusion is treated by using powerful methods that homogenize the environment by the definition of an effective diffusion coefficient (the homogenization process can be perceived as an intelligent averaging of the environment in terms of diffusion coefficients). Continuous limits and effective descriptions require characteristic scales to be bounded and their validity lies far above these bounds (Lesne, 2007). In particular, it is found that in motion through heterogeneous media, anomalous diffusion (subdiffusion) describes the particles' movement over relevant experimental time scales, particularly if the environment is fractal (Saxton, 1994); present macroscopic continuum equations

cannot describe such phenomena. On the other hand, discrete microscopic models, like LGCA, can capture different spatiotemporal scales and they are well-suited for simulating such phenomena.

- Moreover, the discrete structure of the LGCA facilitates the implementation of extremely complicated environments (in the form of tensor fields) without any of the computational problems characterizing continuous models.
- LGCA are perfect examples of parallelizable algorithms. This fact makes them extremely computationally efficient.

While defining a new LGCA model, the following points have to be treated with special caution:

- An important aspect of the LGCA modeling approach to multiscale phenomena is the correct choice of the spatiotemporal scales. In particular, cell migration in heterogeneous environments involves various processes at different spatiotemporal scales. The LGCA models considered in this paper focus at the cellular scale. Moreover, intracellular effects are incorporated in a coarse-grained manner. If one attempts to deal with smaller scales explicitly, extensions of the suggested models are required. In the LGCA (and LBE) literature one can find various solutions for multiscale phenomena, as extension of the state space or multigrid techniques (Succi, 2001).
- An arbitrary choice of a lattice can introduce artificial anisotropies in the evolution of some macroscopic quantities, e.g., in the square lattice the 4th rank tensor is anisotropic (for instance the macroscopic momentum and pressure tensor). These problems can be solved by the use of hexagonal lattices (Frisch *et al.*, 1987) in 2D and the FCHC (Face Centered HyperCubic) lattices (Succi, 2001).
- The simplified LGCA dynamics and the discreteness of space and time can introduce spurious staggered invariants, which can produce undesired artifacts like spurious conservation laws (Kadanoff *et al.*, 1989).

In this paper, we have analyzed LGCA models for nonproliferative cell motion in static heterogeneous environments. A straightforward extension of our models would be the explicit modeling of dynamic cell–environment interactions, i.e., proteolytic activity and ECM remodeling. The works of Chauviere *et al.* (2007) and Hillen (2006) have modeled and analyzed the interactions of cell populations and dynamic environment in terms of kinetic models and transport equations, respectively. The models have shown self-organization of a random environment into a network that facilitates cell motion. However, these models are mass-conserving (the cell population is not changing in time). Our goal is to model and analyze similar situations with LGCA for a cell population that interacts with its environment and changes its density along time.

Moreover, the introduction of proliferation allows the triggering of traveling fronts. In Hatzikirou *et al.* (2007) we have modeled tumor invasion as a diffusive, proliferative cell population (no explicit consideration of any environment) and we have calculated the speed of the traveling front in terms of microscopically accessible parameters. It

would be interesting to analyze the environmental effect on the speed of the tumor expansion.

A further interesting aspect of LGCA is that the corresponding Lattice Boltzmann Equations (LBE) can be used as efficient numerical solvers of continuous macroscopic equations. In particular, LBEs which are LGCA with continuous state space, have been used as efficient solvers of Navier–Stokes equations for fluid dynamical problems (Succi, 2001). In an on-going project with K. Painter (Hatzikirou *et al.*, 2007), we try to use LBE models as efficient numerical solvers of kinetic models.

Note that apart from cell migration, the microenvironment plays an important role in the evolutionary dynamics (as a kind of selective pressure) of evolving cellular systems, like cancer (Anderson *et al.*, 2006; Basanta *et al.*, 2007). It is evident that a profound understanding of microenvironmental effects could help not only to understand developmental processes but also to design novel therapies for diseases such as cancer.

In summary, a module-oriented modeling approach, as demonstrated in this paper, hopefully contributes to an understanding of migration strategies which contribute to the astonishing phenomena of embryonic morphogenesis, immune defense, wound repair and cancer evolution.

Acknowledgments

Appendix A

A lattice-gas cellular automaton is a cellular automaton with a particular state space and dynamics. Therefore, we start with the introduction of cellular automata which are defined as a class of spatially and temporally discrete dynamical systems based on local interactions. In particular, a cellular automaton is a 4-tuple $(\mathcal{L}, \mathcal{E}, \mathcal{N}, \mathcal{R})$, where

- $\mathcal{L}$ is an infinite regular lattice of nodes (discrete space),
- $\mathcal{E}$ is a finite set of states (discrete state space); each node $r \in \mathcal{L}$ is assigned a state $s \in \mathcal{E}$,

- $\mathcal{N}$ is a finite set of neighbors, indicating the position of one node relative to another node on the lattice $\mathcal{L}$ (neighborhood); Moore and von Neumann neighborhoods are typical neighborhoods on the square lattice,
- $\mathcal{R}$ is a deterministic or probabilistic map

$$\mathcal{R} : \mathcal{E}^{|\mathcal{N}|} \to \mathcal{E},$$
$$\{s_i\}_{i \in \mathcal{N}} \; \mapsto s,$$

which assigns a new state to a node depending on the states of all its neighbors indicated by $\mathcal{N}$ (local rule).

The temporal evolution of a cellular automaton is defined by applying the function $\mathcal{R}$ synchronously to all nodes of the lattice $\mathcal{L}$ (homogeneity in space and time).

A.1. States in Lattice-Gas Cellular Automata

In lattice-gas cellular automata, velocity channels $(r, \mathbf{c}_i)$, $\mathbf{c}_i \in \mathcal{N}_b(r)$, $i = 1, \dots, b$, are associated with each node r of the lattice. Here, b is the *coordination number* (for details see below). In addition, a variable number $\beta \in \mathbb{N}_0$ of rest channels (zero-velocity channels), $(r, \mathbf{c}_i)$, $b < i \leqslant b + \beta$, with $\mathbf{c}_i = \{0\}^\beta$ may be introduced. Furthermore, an exclusion principle is imposed. This requires, that not more than one particle can be at the same node within the same channel. As a consequence, each node r can host up to $\tilde{b} = b + \beta$ particles, which are distributed in different channels $(r, \mathbf{c}_i)$ with at most one particle per channel. Therefore, state $s(r)$ is given by

$$s(r) = \big(\eta_1(r), \dots, \eta_{\tilde{b}}(r)\big) =: \boldsymbol{\eta}(r),$$

where $\boldsymbol{\eta}(r)$ is called node configuration and $\eta_i(r) \in \{0, 1\}$, $i = 1, \dots, \tilde{b}$ are called occupation numbers which are Boolean variables that indicate the presence ($\eta_i(r) = 1$) or absence ($\eta_i(r) = 0$) of a particle in the respective channel $(r, \mathbf{c}_i)$. Therefore, the set of elementary states $\mathcal{E}$ of a single node is given by

$$\mathcal{E} = \{0, 1\}^{\tilde{b}}.$$

For any node $r \in \mathcal{L}$, the nearest lattice neighborhood $\mathcal{N}_b(r)$ is a finite list of neighboring nodes and is defined as

$$\mathcal{N}_b(r) := \{r + \mathbf{c}_i \colon \mathbf{c}_i \in \mathcal{N}_b, \; i = 1, \dots, b\},$$

where b is the *coordination number*, i.e., the number of nearest neighbors on the lattice.

Fig. 1 gives an example of the representation of a node on a two-dimensional lattice with $b = 4$ and $\beta = 1$, i.e., $\tilde{b} = 5$.

In multicomponent LGCA, ς different types (σ) of particles reside on separate lattices ($\mathcal{L}_\sigma$) and the exclusion principle is applied independently to each lattice. The

state variable is given by

$$s(r) = \boldsymbol{\eta}(r) = \left(\boldsymbol{\eta}_\sigma(r)\right)_{\sigma=1}^{\varsigma} = \left(\eta_{\sigma,1}(r), \ldots, \eta_{\sigma,\tilde{b}}(r)\right)_{\sigma=1}^{\varsigma} \in \mathcal{E} = \{0, 1\}^{\tilde{b}\varsigma}.$$

A.2. Dynamics in Lattice-Gas Cellular Automata

The dynamics of a LGCA arises from repetitive application of superpositions of local (probabilistic) *interaction* and deterministic *propagation* (migration) steps applied simultaneously at all lattice nodes at each discrete time step. The definitions of these steps have to satisfy the exclusion principle, i.e., two or more particles are not allowed to occupy the same channel.

According to a model-specific *interaction* rule ($\mathcal{R}^C$), particles can change channels (see Fig. 2) and/or are created or destroyed. The temporal evolution of a state $s(r, k) = \boldsymbol{\eta}(r, k) \in \{0, 1\}^{\tilde{b}}$ in a LGCA is determined by the temporal evolution of the occupation numbers $\eta_i(r, k)$ for each $i \in \{1, \ldots, \tilde{b}\}$ at node r and time k. Accordingly, the preinteraction state $\eta_i(r, k)$ is replaced by the postinteraction state $\eta_i^C(r, k)$ determined by

$$\eta_i^C(r, k) = \mathcal{R}_i^C\left(\boldsymbol{\eta}_{\mathcal{N}(r)}(k)\right), \tag{21}$$

$$\mathcal{R}^C\left(\boldsymbol{\eta}_{\mathcal{N}(r)}(k)\right) = \left(\mathcal{R}_i^C\left(\boldsymbol{\eta}_{\mathcal{N}(r)}(k)\right)\right)_{i=1}^{\tilde{b}} = z \text{ with probability } P(\boldsymbol{\eta}_{\mathcal{N}(r)}(k) \to z)$$

with $z \in (0, 1)^{\tilde{b}}$ and the time-independent transition probability P.

In the deterministic *propagation* or streaming step (P), all particles are moved simultaneously to nodes in the direction of their velocity, i.e., a particle residing in channel $(r, \mathbf{c}_i)$ at time k is moved to channel $(r + m\mathbf{c}_i, \mathbf{c}_i)$ during one time step (Fig. 3). Here, $m \in \mathbb{N}$ determines the *speed* and $m\mathbf{c}_i$ the *translocation* of the particle. Because all particles residing at velocity channels move the same number m of lattice units, the exclusion principle is maintained. Particles occupying rest channels do not move since they have "zero velocity." In terms of occupation numbers, the state of channel $(r + m\mathbf{c}_i, \mathbf{c}_i)$ after propagation is given by

$$\eta_i^P(r + m\mathbf{c}_i, k+1) = \eta_i(r, k), \quad \mathbf{c}_i \in \mathcal{N}_b. \tag{22}$$

Hence, if only the propagation step would be applied then particles would simply move along straight lines in directions corresponding to particle velocities.

Combining interactive dynamics with propagation, Eqs. (21) and (22) imply that

$$\eta_i^{CP}(r + m\mathbf{c}_i, k) = \eta_i(r + m\mathbf{c}_i, k+1) = \eta_i^C(r, k). \tag{23}$$

This can be rewritten as the *microdynamical difference equations*

$$\begin{aligned}
\mathcal{R}_i^C\left(\boldsymbol{\eta}_{\mathcal{N}(r)}(k)\right) - \eta_i(r, k) &= \eta_i^C(r, k) - \eta_i(r, k) \\
&= \eta_i(r + m\mathbf{c}_i, k+1) - \eta_i(r, k) \\
&=: \mathcal{C}_i\left(\boldsymbol{\eta}_{\mathcal{N}(r)}(k)\right), \quad i = 1, \ldots, \tilde{b},
\end{aligned} \tag{24}$$

where the *change in the occupation numbers* due to interaction is given by

$$
C_i\big(\boldsymbol{\eta}_{\mathcal{N}(r)}(k)\big) = \begin{cases} 1, & \text{creation of a particle in channel } (r, \mathbf{c}_i), \\ 0, & \text{no change in channel } (r, \mathbf{c}_i), \\ -1, & \text{annihilation of a particle in channel } (r, \mathbf{c}_i). \end{cases} \tag{25}
$$

In a multicomponent system with $\sigma = 1, \ldots, \varsigma$ components, Eq. (24) becomes

$$
\eta_{\sigma,i}^{C}(r, k) - \eta_{\sigma,i}(r, k) = \eta_{\sigma,i}(r + m_\sigma \mathbf{c}_i, k + 1) - \eta_{\sigma,i}(r, k)
$$
$$
= C_{\sigma,i}\big(\boldsymbol{\eta}_{\mathcal{N}(r)}(k)\big), \tag{26}
$$

for $i = 1, \ldots, \tilde{b}$, with speeds $m_\sigma \in \mathbb{N}$ for each component $\sigma = 1, \ldots, \varsigma$. Here, the change in the occupation numbers due to interaction is given by

$$
C_{\sigma,i}\big(\boldsymbol{\eta}_{\mathcal{N}(r)}(k)\big) = \begin{cases} 1, & \text{creation of a particle in channel } (r, \mathbf{c}_i)_\sigma, \\ 0, & \text{no change in channel } (r, \mathbf{c}_i)_\sigma, \\ -1, & \text{annihilation of a particle in channel } (r, \mathbf{c}_i)_\sigma, \end{cases} \tag{27}
$$

where $(r, \mathbf{c}_i)_\sigma$ specifies the ith channel associated with node r of the lattice $\mathcal{L}_\sigma$.

Appendix B

In this appendix, we calculate in detail the equilibrium distribution for model I. For the zero-field case, we know that the equilibrium distribution is $f_i^{\text{eq}} = \rho/b = d$. Thus, we can easily find that $h_0 = \ln(\frac{1-d}{d})$. For simplicity of the notation we use f_i instead of f_i^{eq}.

The next step is to expand the equilibrium distribution around $\mathbf{E} = \mathbf{0}$ and we obtain:

$$
f_i = f_i(\mathbf{E} = \mathbf{0}) + \nabla_{\mathbf{E}} f_i \mathbf{E} + \frac{1}{2}\mathbf{E}^T \nabla_{\mathbf{E}}^2 f_i \mathbf{E}. \tag{28}
$$

In the following, we present the detailed calculations. The chain rule gives:

$$
\frac{\partial f_i}{\partial e_\alpha} = \frac{\partial f_i}{\partial x}\frac{\partial x}{\partial e_\alpha}. \tag{29}
$$

Then using Eqs. (9) and (10):

$$
\frac{\partial f_i}{\partial x} = -\frac{e^x}{(1 + e^x)^2} \rightarrow d(d - 1), \tag{30}
$$

$$
\frac{\partial x}{\partial e_\alpha} = \frac{\partial}{\partial e_\alpha}\big(h_0 + h_1 \mathbf{c}_i \mathbf{E} + h_2 \mathbf{E}^2\big) = h_1 c_{i\alpha} + 2h_2 e_\alpha. \tag{31}
$$

For $\mathbf{E} = \mathbf{0}$ we set:

$$
\frac{\partial f_i}{\partial e_\alpha} = d(d - 1)h_1 c_{i\alpha}, \tag{32}
$$

where $\alpha = 1, 2$. Then, we calculate the second-order derivatives:

$$\frac{\partial^2 f_i}{\partial e_\alpha^2} = \frac{\partial}{\partial e_\alpha}\left(\frac{\partial f_i}{\partial x}\frac{\partial x}{\partial e_\alpha}\right) = \frac{\partial^2 f_i}{\partial x \partial e_\alpha}\frac{\partial x}{\partial e_\alpha} + \frac{\partial f_i}{\partial x}\frac{\partial^2 x}{\partial^2 e_\alpha}$$

$$= \frac{\partial^2 f_i}{\partial x^2}\left(\frac{\partial x}{\partial e_\alpha}\right)^2 + \frac{\partial f_i}{\partial x}\frac{\partial^2 x}{\partial e_\alpha^2}. \tag{33}$$

Especially:

$$\frac{\partial^2 f_i}{\partial x^2} = \frac{e^x(e^x - 1)}{(1 + e^x)^3} = d(d - 1)(2d - 1), \tag{34}$$

$$\frac{\partial^2 x}{\partial e_\alpha^2} = 2h_2. \tag{35}$$

Thus, relation (33) reads:

$$\frac{\partial^2 f_i}{\partial e_\alpha^2} = d(d - 1)(2d - 1)h_1^2 c_{i\alpha} + d(d - 1)2h_2. \tag{36}$$

For the case $\alpha \neq \beta$ $(\alpha, \beta = 1, 2)$, we have:

$$\frac{\partial^2 f_i}{\partial e_\alpha \partial e_\beta} = \frac{\partial}{\partial e_\beta}\left(\frac{\partial f_i}{\partial x}\frac{\partial x}{\partial e_\alpha}\right) = \frac{\partial^2 f_i}{\partial x \partial e_\beta}\frac{\partial x}{\partial e_\alpha} + \frac{\partial f_i}{\partial x}\frac{\partial^2 x}{\partial e_\alpha \partial e_\beta}$$

$$= \frac{\partial^2 f_i}{\partial x^2}\frac{\partial x}{\partial e_\alpha}\frac{\partial x}{\partial e_\beta} + \frac{\partial f_i}{\partial x}\frac{\partial^2 x}{\partial e_\alpha \partial e_\beta}. \tag{37}$$

We can easily derive:

$$\frac{\partial^2 x}{\partial e_\alpha \partial e_\beta} = 0. \tag{38}$$

Thus, Eq. (37) becomes:

$$\frac{\partial^2 f_i}{\partial e_\alpha \partial e_\beta} = d(d - 1)(2d - 1)h_1^2 c_{i\alpha} c_{i\beta}. \tag{39}$$

Finally, the equilibrium distribution is:

$$f_i = d + d(d - 1)h_1 \mathbf{c}_i \mathbf{E} + \frac{1}{2}d(d - 1)(2d - 1)h_1^2 \sum_\alpha c_{i\alpha}^2 e_\alpha^2 + d(d - 1)h_2 \mathbf{E}^2. \tag{40}$$

In the last relation, we have to determine the free parameters h_1, h_2. Using the mass conservation law, we can find a relation between h_1 and h_2:

$$\rho = \sum_{i=1}^{b} f_i$$

$$= \underbrace{\sum_i d}_{\rho} + \underbrace{d(d-1)h_1 \sum_i \mathbf{c}_i \mathbf{E}}_{0} + \underbrace{\frac{1}{2}d(d-1)(2d-1)h_1^2 \sum_i \sum_\alpha c_{i\alpha}^2 e_\alpha^2}_{\frac{b}{2}\mathbf{E}^2}$$

$$+ d(d-1)h_2 \sum_i h_2 \mathbf{E}^2. \tag{41}$$

For any choice of the lattice, we find:

$$h_2 = \frac{1-2d}{4}h_1^2. \tag{42}$$

Finally, the equilibrium distribution can be explicitly calculated for small driving fields:

$$f_i = d + d(d-1)h_1 \mathbf{c}_i \mathbf{E} + \frac{1}{2}d(d-1)(2d-1)h_1^2 Q_{\alpha\beta} e_\alpha e_\beta, \tag{43}$$

where $Q_{\alpha\beta} = c_{i\alpha}c_{i\beta} - \frac{1}{2}\delta_{\alpha\beta}$ is a second-order tensor.

We now calculate the mean flux, in order to obtain the linear response relation:

$$\langle \mathbf{J}(\eta^C) \rangle = \sum_i c_{i\alpha} f_i = \frac{b}{2}d(d-1)h_1 \mathbf{E}. \tag{44}$$

Thus, the susceptibility reads:

$$\chi = \frac{1}{2}bd(d-1)h_1 = -\frac{1}{2}bg_{eq}h_1. \tag{45}$$

Appendix C

In this appendix, we present details of the calculation of the equilibrium distribution for model II. To simplify the calculations, we restrict ourselves to the case of the square lattice ($b = 4$).

Using the mass conservation law, allows us to calculate the relation between h_1, h_2.

$$\rho = \sum_{i=1}^{b} f_i$$

$$= \underbrace{\sum_i d}_{\rho} + d(d-1)h_1 \sum_i |\mathbf{c}_i| \mathbf{E} + \frac{1}{2}d(d-1)(2d-1)h_1^2 \underbrace{\sum_i \sum_\alpha c_{i\alpha}^2 e_\alpha^2}_{\frac{b}{2}E^2}$$

$$+ d(d-1)(2d-1)h_1^2 \underbrace{\sum_i |c_{i\alpha}c_{i\beta}|e_\alpha e_\beta}_{\frac{b}{2}\delta_{\alpha\beta}e_\alpha e_\beta} + d(d-1)h_2 \sum_i \mathbf{E}^2. \qquad (46)$$

Finally, the previous equation becomes:

$$2d(d-1)h_1 \sum_\alpha e_\alpha + d(d-1)(2d-1)h_1^2\mathbf{E}^2 + 4d(d-1)h_2\mathbf{E}^2 = 0, \qquad (47)$$

and we find:

$$h_2 = \frac{1-2d}{4}h_1^2 - \frac{1}{2}\frac{e_1+e_2}{e_1^2+e_2^2}h_1. \qquad (48)$$

Appendix D

In this appendix, we estimate the free parameter h_1 for model II.

The field $\mathbf{E}$ induces a spatially homogeneous deviation from the field-free equilibrium state $f_i(\mathbf{r}|\mathbf{E}=\mathbf{0}) = f_{eq}$ of the form:

$$f_i(\mathbf{r}|\mathbf{E}) = f_{eq} + \delta f_i(\mathbf{E}). \qquad (49)$$

We denote the transition probability as $P(\eta \to \eta^C) = A_{\eta\eta^C}$. The average flux is given by:

$$\langle \mathbf{J}(\eta^C) \rangle = \sum_{i=1}^b \mathbf{c}_i \delta f_i(\mathbf{E}). \qquad (50)$$

For small $\mathbf{E}$ we expand Eq. (4) as:

$$A_{\eta\eta^C}(\mathbf{E}) \simeq A_{\eta\eta^C}(0)\{1 + [|\mathbf{J}(\eta^C)| - |\overline{\mathbf{J}(\eta^C)}|]\mathbf{E}\}, \qquad (51)$$

where we have defined the expectation value of $\mathbf{J}(\eta^C)$ averaged over all possible outcomes η^C of a collision taking place in a field-free situation:

$$|\overline{\mathbf{J}(\eta^C)}| = \sum_{\eta^C}|\mathbf{J}(\eta^C)|A_{\eta\eta^C}(0). \qquad (52)$$

In the mean-field approximation the deviations $\delta f(\mathbf{E})$ are implicitly defined as stationary solutions of the nonlinear Boltzmann equation for a given $\mathbf{E}$, i.e.

$$\Omega_i^{10}[f_{eq} + \delta f_i(\mathbf{E})] = 0. \qquad (53)$$

Here the nonlinear Boltzmann operator is defined by:

$$\Omega_i^{10}(\mathbf{r}, t) = \langle \eta_i^C(\mathbf{r}, t) - \eta_i(\mathbf{r}, t) \rangle_{MF}$$
$$= \sum_{\eta^C} \sum_{\eta} [\eta_i^C(\mathbf{r}, t) - \eta_i(\mathbf{r}, t)] A_{\eta \eta^C}(\mathbf{E}) F(\eta, \mathbf{r}, t), \tag{54}$$

where the factorized single node distribution is defined as:

$$F(\eta, \mathbf{r}, t) = \prod_i [f_i(\mathbf{r}, t)]^{\eta_i} [1 - f_i(\mathbf{r}, t)]^{1-\eta_i}. \tag{55}$$

Linearizing around the equilibrium distribution yields:

$$\Omega_i^{10} [f_{eq} + \delta f_i(\mathbf{E})] = \Omega_i^{10}(f_i) + \sum_j \Omega_{ij}^{11}(f_{eq}) \delta f_j(\mathbf{E}), \tag{56}$$

where $\Omega_{ij}^{11} = \frac{\partial \Omega_i^{10}}{\partial f_j}$. Moreover:

$$\Omega_i^{10}(f_{eq}) = \sum_{\eta^C, \eta} (\eta_i^C - \eta_i) \{ 1 + [|\mathbf{J}(\eta^C)| - |\overline{\mathbf{J}(\eta^C)}|] \mathbf{E} \} A_{\eta \eta^C}(0) F(\eta). \tag{57}$$

Using the relations $\sum (\eta_i^C - \eta_i) A_{\eta \eta^C}(0) F(\eta) = 0$ and $\sum (\eta_i^C - \eta_i) |\overline{\mathbf{J}(\eta^C)}| A_{\eta \eta^C}(0) \times F(\eta) = 0$, we obtain:

$$\Omega_i^{10}(f_{eq}) = \langle (\eta_i^C - \eta_i) |\mathbf{J}(\eta^C)| \rangle \mathbf{E}. \tag{58}$$

Around $\mathbf{E} = \mathbf{0}$ we set:

$$\sum_j \Omega_{ij}^{11}(f_{eq}) \delta f_j(\mathbf{E}) + \langle (\eta_i^C - \eta_i) |\mathbf{J}(\eta^C)| \rangle_{MF} \mathbf{E} = 0. \tag{59}$$

Solving the above equation involves the inversion of the symmetric matrix $\Omega_{ij}^{11} = 1/b - \delta_{ij}$. It can be proven that the linearized Boltzmann operator looks like:

$$\Omega_{ij}^{11} = \left\langle (\delta \eta_i^C - \delta \eta_i) \frac{\delta \eta_j}{g_{eq}} \right\rangle = \frac{1}{g_{eq}} (\langle \delta \eta_i^C, \delta \eta_j \rangle - \langle \delta \eta_i, \delta \eta_j \rangle), \tag{60}$$

where $\delta \eta_i = \eta_i - f_{eq}$ and the single particle fluctuation $g_{eq} = f_{eq}(1 - f_{eq})$. For the second term of the last part of Eq. (60), we have $\langle \delta \eta_i, \delta \eta_j \rangle = \delta_{ij} g_{eq}$. To evaluate the first term, we note that the outcome of the collision rule only depends on $\eta(\mathbf{r})$ through $\rho(\mathbf{r})$, so that the first quantity does not depend on the i and j and

$$\langle \delta \eta_i^C, \delta \eta_j \rangle = \frac{1}{b^2} \langle [\delta \rho(\mathbf{r})]^2 \rangle = \frac{1}{b} g_{eq}, \tag{61}$$

where we have used $\rho(\eta) = \rho(\eta^C)$. Thus Eq. (60) takes the value $(1/b - \delta_{ij})$.

Returning to the calculation of the generalized inverse of Ω^{11}, we observe that its null space is spanned by the vector $(\overbrace{1, \ldots, 1}^{b})$, which corresponds to the conservation

of particles

$$\sum_i \delta f_i(\mathbf{E}) = 0. \tag{62}$$

The relation satisfies the solvability condition of the Fredholm alternative for Eq. (59), which enables us to invert the matrix within the orthogonal complement of the null space. With some linear algebra, we can prove that the generalized inverse $[\Omega^{11}]^{-1}$ has the same eigenvectors but inverse eigenvalues as the original matrix Ω^{11}. In particular, it can be verified that since $\mathbf{c}_{\alpha i}$, $\alpha = 1, 2$ (where 1, 2 stands for x- and y-axis, respectively) are eigenvectors of Ω^{11} with eigenvalue -1, we have

$$\sum_j [\Omega_{ij}^{11}]^{-1} c_{aj} = -c_{ai}. \tag{63}$$

Now we can calculate the flux of particles for one direction:

$$\langle J_{a^+}(\eta^C)\rangle = -\sum_j c_{aj} [\Omega_{ij}^{11}]^{-1} \langle (\eta_i^C - \eta_i) | \mathbf{J}_\beta(\eta^C)| \rangle e_a$$
$$= c_{ai} \langle (\eta_i^C - \eta_i) | \mathbf{J}_\beta(\eta^C)| \rangle e_a. \tag{64}$$

Calculating in detail the last relation:

$$c_{ai} \langle (\eta_i^C - \eta_i) | \mathbf{J}_\beta(\eta^C)| \rangle = \tag{65}$$

$$= c_{ai} \sum_j |c_{\beta j}| \langle (\delta\eta_i^C - \delta\eta_i)\delta\eta_j^C \rangle \tag{66}$$

$$= \frac{1}{2} g_{eq} c_{ai}. \tag{67}$$

The observable quantity that we want to calculate for the second rule is:

$$\left| \langle \mathbf{J}_{x^+}(\eta^C)\rangle - \langle \mathbf{J}_{y^+}(\eta^C)\rangle \right| = \frac{1}{2} g_{eq}|e_1 - e_2|, \tag{68}$$

since $c_{11} = c_{22} = 1$.

References

Alexander, F. J., Edrei, I., Garrido, P. L., and Lebowitz, J. L. (1992). Phase transitions in a probabilistic cellular automaton: Growth kinetics and critical properties. *J. Stat. Phys.* **68**(3/4), 497–514.

Anderson, A. R., Weaver, A. M., Cummings, P. T., and Quaranta, V. (2006). Tumor morphology and phenotypic evolution driven by selective pressure from the microenvironment. *Cell* **127**(5), 905–915.

Basanta, D., Simon, M., Hatzikirou, H., and Deutsch, A. (2007). Evolutionary game theory elucidates the role of glycolysis in glioma progression and invasion. Cancer Res. submitted for publication.

Bru, A., Albertos, S., Subiza, J. L., Lopez Garcia-Asenjo, J., and Bru, I. (2003). The universal dynamics of tumor growth. *Biophys. J.* **85**, 2948–2961.

Bussemaker, H. (1996). Analysis of a pattern forming lattice gas automaton: Mean field theory and beyond. *Phys. Rev. E* **53**(2), 1644–1661.

Byrne, H., and Preziosi, H. (2003). Modeling solid tumor growth using the theory of mixtures. *Math. Med. Biol.* **20**(4), 341–366.

Carter, S. B. (1965). Principles of cell motility: The direction of cell movement and cancer invasion. *Nature* **208**(5016), 1183–1187.

Chauviere, A., Hillen, T., and Preziosi L. (2007). Modeling the motion of a cell population in the extracellular matrix. *Discr. Cont. Dyn. Syst.* (to appear).

Chopard, B., and Droz, M. (1998). "Cellular Automata Modeling of Physical Systems." Cambridge Univ. Press, Cambridge.

Dallon, J. C., Sherratt, J. A., and Maini, P. K. (2001). Modeling the effects of transforming growth factor on extracellular alignment in dermal wound repair. *Wound Rep. Reg.* **9**, 278–286.

De Franciscis, S., Hatzikirou, H., and Deutsch, A. (2007). Evaluation of discrete models of avascular tumor growth by means of fractal scaling analysis (preprint).

Deutsch, A., and Dormann, S. (2005). "Cellular Automaton Modeling of Biological Pattern Formation." Birkhäuser, Boston.

Dickinson, R. B., and Tranquillo, R. T. (1993). A stochastic model for cell random motility and haptotaxis based on adhesion receptor fluctuations. *J. Math. Biol.* **31**, 563–600.

Dickinson, R. B., and Tranquillo, R. T. (1995). Transport equations and cell movement indices based on single cell properties. *SIAM J. Appl. Math.* **55**(5), 1419–1454.

Dolak, Y., and Schmeiser, C. (2005). Kinetic models for chemotaxis: Hydrodynamic limits and spatiotemporal mechanics. *J. Math. Biol.* **51**, 595–615.

Friedl, P. (2004). Prespecification and plasticity: Shifting mechanisms of cell migration. *Curr. Opin. Cell. Biol.* **16**(1), 14–23.

Friedl, P., and Broecker, E. B. (2000). The biology of cell locomotion within a three dimensional extracellular matrix. *Cell Motil. Life Sci.* **57**, 41–64.

Friedl, P., and Wolf, K. (2003). Tumor-cell invasion and migration: Diversity and escape mechanisms. *Nat. Rev.* **3**, 362–374.

Frisch, U., d'Humieres, D., Hasslacher, B., Lallemand, P., Pomeau, Y., and Rivet, J. -P. (1987). Lattice gas hydrodynamics in two and three dimensions. *Compl. Syst.* **1**, 649–707.

Galle, J., Aust, G., Schaller, G., Beyer, T., and Drasdo, D. (2006). Individual cell-based models of the spatial-temporal organization of multicellular systems—achievements and limitations. *Cytom. Part A* **69A**(7), 704–710.

Grima, R. (2007). Directed cell migration in the presence of obstacles. *Theor. Biol. Med. Model.* **4**, 2.

Hatzikirou, H., Brusch, L., Schaller, C., Simon, M., and Deutsch, A. (2007). Characterization of traveling front behavior in a lattice gas cellular automaton model of glioma invasion. *Math. Comp. Mod.* (in print).

Hatzikirou, H., Deutsch, A., Schaller, C., Simon, M., and Swanson, K. (2005). Mathematical modeling of glioblastoma tumor development: A review. *Math. Mod. Meth. Appl. Sci.* **15**(11), 1779–1794.

Hatzikirou, H., Painter, K., and Deutsch, A. (2007). Numerical solvers of transport equations modeling individual cell motion. *J. Math. Biol.* (in preparation).

Hillen, T. (2006). (M5) Mesoscopic and macroscopic models for mesenchymal motion. *J. Math. Biol.* **53**, 585–616.

Kadanoff, L. P., McNamara, G. R., and Zanetti, G. (1989). From automata to fluid flow: Comparisons of simulation and theory. *Phys. Rev. A* **40**, 4527–4541.

Keller, E. F., and Segel, L. A. (1971). Traveling bands of chemotactic bacteria: A theoretical analysis. *J. Theor. Biol.* **30**, 235–248.

Lesne, A. (2007). Discrete vs continuous controversy in physics. *Math. Struct. Comp. Sci.* (in print).

Liggett, T. M. (1985). "Interacting Particle Systems." Springer-Verlag, Berlin.

McCarthy, J. B., and Furcht, L. T. (1984). Laminin and fibronectin promote the haptotactic migration of B16 mouse melanoma cells. *J. Cell Biol.* **98**(4), 1474–1480.

Murray, J. D., Oster, G. F., and Harris, A. K. (1983). A mechanical model for mesenchymal morphogenesis. *J. Math. Biol.* **17**, 125–129.

Newman, T. J., and Grima, R. (2004). Many-body theory of chemotactic cell–cell interactions. *Phys. Rev. E* **70**, 051916.

Okubo, A., and Levin, S. A. (2002). "Diffusion and Ecological Problems: Modern Perspectives." Springer-Verlag, New York.

Othmer, H. G., and Stevens, A. (1997). Aggregation, blowup and collapse: The ABC's of taxis in reinforced random walks. *SIAM J. Appl. Math.* **57**, 1044–1081.

Othmer, H. G., Dunbar, S. R., and Alt, W. (1988). Models of dispersal in biological systems. *J. Math. Biol.* **26**, 263–298.

Palecek, S. P., Loftus, J. C., Ginsberg, M. H., Lauffenburger, D. A., and Horwitz, A. F. (1997). Integrin-ligand binding governs cell-substratum adhesiveness. *Nature* **388**(6638), 210.

Peruani, F., and Morelli, L. (2007). Self-propelled particles with fluctuating speed. *Phys. Rev. Lett.* **99**, 010602.

Saxton, M. (1994). Anomalous diffusion due to obstacles: A Monte Carlo study. *Biophys. J.* **66**, 394–401.

Schweitzer, F. (2003). "Brownian Agents and Active Particles." Springer-Verlag, Berlin.

Succi, S. (2001). "The Lattice Boltzmann Equation: For Fluid Dynamics and Beyond." "Numerical Mathematics and Scientific Computation." Oxford Univ. Press, Oxford, NY.

Swanson, K. R., Alvord Jr., E. C., and Murray, J. D. (2002). Virtual brain tumors (gliomas) enhance the reality of medical imaging and highlights inadequacies of current therapy. *Brit. J. Canc.* **86**, 14–18.

Turing, A. M. (1952). The chemical basis of morphogenesis. *Philos. Trans. R. Soc. London B* **237**, 37–72.

Zaman, M. H., Matsudaira, P., and Lauffenburger, D. A. (2006). Understanding effects of matrix protease and matrix organization on directional persistence and translational speed in three-dimensional cell migration. *Ann. Biomed. Eng.* **35**(1), 91–100.